Genetic screen for suppression of transcriptional interference identifies a gain-of-function mutation in Pol2 termination factor Seb1

Beate Schwer[a,1], Angad Garg[b], Agata Jacewicz[b], and Stewart Shuman[b,1]

[a]Department of Microbiology and Immunology, Weill Cornell Medical College, New York, NY 10065; and [b]Molecular Biology Program, Sloan Kettering Institute, New York, NY 10065

Edited by Fred M. Winston, Harvard Medical School, Boston, MA, and approved July 2, 2021 (received for review April 29, 2021)

The system of long noncoding RNA (lncRNA)–mediated transcriptional interference that represses fission yeast phosphate homoeostasis gene *pho1* provides a sensitive readout of genetic influences on cotranscriptional 3′-processing and termination and a tool for discovery of regulators of this phase of the Pol2 transcription cycle. Here, we conducted a genetic screen for relief of transcriptional interference that unveiled a mechanism by which Pol2 termination is enhanced via a gain-of-function mutation, G476S, in the RNA-binding domain of an essential termination factor, Seb1. The genetic and physical evidence for gain-of-function is compelling: 1) *seb1-G476S* de-represses *pho1* and *tgp1*, both of which are subject to lncRNA-mediated transcriptional interference; 2) *seb1-G476S* elicits precocious lncRNA transcription termination in response to lncRNA 5′-proximal poly(A) signals; 3) *seb1-G476S* derepression of *pho1* is effaced by loss-of-function mutations in cleavage and polyadenylation factor (CPF) subunits and termination factor Rhn1; 4) synthetic lethality of *seb1-G476S* with *pho1* derepressive mutants *rpb1-CTD-S7A* and *aps1*Δ is rescued by CPF/Rhn1 loss-of-function alleles; and 5) *seb1-G476S* elicits an upstream shift in poly(A) site preference in several messenger RNA genes. A crystal structure of the Seb1-G476S RNA-binding domain indicates potential for gain of contacts from Ser476 to RNA nucleobases. To our knowledge, this is a unique instance of a gain-of-function phenotype in a eukaryal transcription termination protein.

transcription termination | RNA 3′-processing | phosphate homeostasis | CTD code | inositol pyrophosphates

Termination of transcription by RNA polymerase II (Pol2) typically occurs downstream of sites of nascent RNA 3′ cleavage and polyadenylation. The prevailing "torpedo model" holds that the 5′-phosphate nascent RNA terminus generated by endonuclease cleavage permits ingress of a processive nuclear 5′ exonuclease that digests the nascent RNA and elicits termination when it "catches up" to elongating Pol2 (1, 2). Timely 3′-processing and Pol2 termination delimits the distal margins of transcription units and avoids transcription interference with the expression of neighboring genes (3). The Pol2 elongation complex and associated elongation factors, the cleavage and polyadenylation apparatus, and postcleavage termination factors together comprise a large physical and functional target for regulating 3′ end formation and termination.

Interference occurs when transcription initiating from an upstream promoter quashes initiation at a cooriented downstream promoter (4). In eukaryal genomes, in which transcription units specifying messenger RNAs (mRNAs) and long noncoding (lnc) RNAs are interspersed, there are many occasions for lncRNA synthesis to negatively impact a flanking protein-coding gene (5). This mode of control is exemplified in fission yeast, in which lncRNA interference with mRNA expression is the basis for transcriptional control of phosphate homeostasis. To wit, the fission yeast phosphate (*PHO*) regulon (6) comprises three phosphate acquisition genes—*pho1* (cell surface acid phosphatase), *pho84* (inorganic phosphate transporter), and *tgp1* (glycerophosphodiester transporter)—each of which is repressed during growth in phosphate-rich medium by transcription in *cis* of a 5′ flanking lncRNA, these being *prt(nc-pho1)*, *prt2*, and *nc-tgp1*, respectively (reviewed in ref. 7). lncRNA transcription traversing the *PHO* mRNA promoters evicts the *PHO* gene-activating transcription factor Pho7 from its DNA binding sites (8). The *PHO* genes are derepressed by genetic maneuvers that encourage precocious lncRNA 3′-processing/termination upstream of the *PHO* mRNA promoters, thereby allowing Pho7 binding (9–15). Conversely, the *PHO* genes are hyperrepressed in cells bearing loss-of-function mutations in components of the 3′-processing/termination machinery (12, 13).

It is of particular interest that lncRNA termination is influenced by the Pol2 carboxyl-terminal domain (CTD) code. The CTD of the Pol2 Rpb1 subunit consists of tandem repeats of a consensus heptapeptide sequence, $Y^1S^2P^3T^4S^5P^6S^7$, that acts as a platform to engage proteins that govern transcription and catalyze mRNA processing. The CTD primary structure, which is dynamically remodeled by serine, threonine, and tyrosine phosphorylation, conveys information about the status of the Pol2 transcription apparatus—a CTD code—that is read by CTD-interacting proteins (16–19). Replacement of all fission yeast CTD Ser7 residues with alanine results in derepression of *pho1*, *pho84*, and *tgp1* expression in phosphate-replete cells, whereas replacement of all Thr4 residues with alanine causes *pho1* and *pho84* hyperrepression (12).

Significance

Long noncoding RNA (lncRNA) transcriptional interference with the synthesis of downstream messenger RNAs underlies regulated biological responses of yeast cells to nutrient availability. For example, expression of the phosphate (*PHO*) regulon in phosphate-replete fission yeast cells is tunable by genetic manipulations that favor or disfavor precocious lncRNA 3′-processing/termination. A forward genetic screen for relief of lncRNA interference with *pho1* expression uncovered a mutation G476S in the RNA-binding domain of essential termination factor Seb1 that evokes precocious lncRNA termination in response to 5′-proximal poly(A) sites in a manner dependent on cleavage and polyadenylation factor CPF, termination factor Rhn1, and inositol pyrophosphate synthesis. Multiple lines of evidence point to Seb1-G476S as a unique gain-of-function mutation in a Pol2 transcription termination factor.

Author contributions: B.S., A.G., A.J., and S.S. designed research; B.S., A.G., and A.J. performed research; B.S., A.G., A.J., and S.S. analyzed data; and B.S. and S.S. wrote the paper.

The authors declare no competing interest.

This article is a PNAS Direct Submission.

[1]To whom correspondence may be addressed. Email: s-shuman@ski.mskcc.org or bschwer@med.cornell.edu.

This article contains supporting information online at https://www.pnas.org/lookup/suppl/doi:10.1073/pnas.2108105118/-/DCSupplemental.

Published August 13, 2021.

Several lines of evidence connect the impact of CTD mutations on *PHO* gene expression to the protein factors that direct cotranscriptional RNA 3′-processing and Pol2 termination. Cleavage and polyadenylation factor (CPF) is a 13-subunit protein assembly responsible for the cleavage and 3′-polyadenylation of nascent Pol2 transcripts that precedes termination (20). Eight of the fission yeast CPF subunits, including the cleavage endonuclease Ysh1 and the poly(A) polymerase Pla1, are essential for viability. Five of the CPF subunits are dispensable for growth: Ctf1, Ssu72 (a phosphoprotein phosphatase that acts on the CTD), Dis2 (a phosphoprotein phosphatase), Ppn1, and Swd22. Seb1 and Rhn1 are transcription termination factors that bind the phospho-CTD (21). Whereas Seb1 is essential in fission yeast, Rhn1 is not. The derepression of *pho1* by the *CTD-S7A* mutation was negated by deletion or loss-of-function mutations of CPF subunits Ctf1, Ssu72, Ppn1, Swd22, and Dis2 and termination factor Rhn1 (12). These CPF/Rhn1 mutations per se caused hyperrepression of *pho1*, akin to the effects of *CTD-T4A* (12). The finding that *CTD-T4A* is synthetically lethal with *ppn1*Δ and *swd22*Δ indicates that Thr4 and the Ppn1•Swd22 module of CPF play important, albeit functionally redundant, roles in promoting Pol2 termination (12).

To understand how the *CTD-T4A* mutation affects interference and to potentially identify agents of *prt* lncRNA transcription and transcription termination, we recently undertook a genetic screen in mutagenized *CTD-T4A* cells for suppressors of the *pho1* hyperrepressed state (22). Using a chromogenic overlay assay to gauge acid phosphatase activity of individual colonies, we obtained a collection of candidate suppressor mutants that had elevated Pho1 activity vis-à-vis the parental *CTD-T4A* cells. The candidates underwent several rounds of backcrossing to affirm single-gene segregation of the increased Pho1 phenotype, which was verified by quantitative assays of Pho1 activity. Analysis of 18 independent *STF* (suppressor of threonine four) isolates revealed, in every case, a mutation in the carboxyl-terminal pyrophosphatase domain of the enzyme Asp1 (22), a central agent of inositol pyrophosphate (IPP) metabolism. Asp1 is a bifunctional IPP kinase/pyrophosphatase that interconverts 5-IP7 and 1,5-IP8 (23, 24). We had shown that an active site mutation in the N-terminal kinase domain that abolishes IP8 synthesis results in hyperrepression of *pho1* expression, while an active site mutation in the pyrophosphatase domain (that elevates IP8 levels) causes *pho1* derepression in a manner that requires CPF subunits and Rhn1 (25). Transcriptome profiling of two of the new *STF* strains showed that all three *PHO* regulon genes were coordinately up-regulated vis-à-vis the parental *T4A* strain. Moreover, whereas these two *asp1-STF* alleles were lethal in a wild-type CTD background, they were

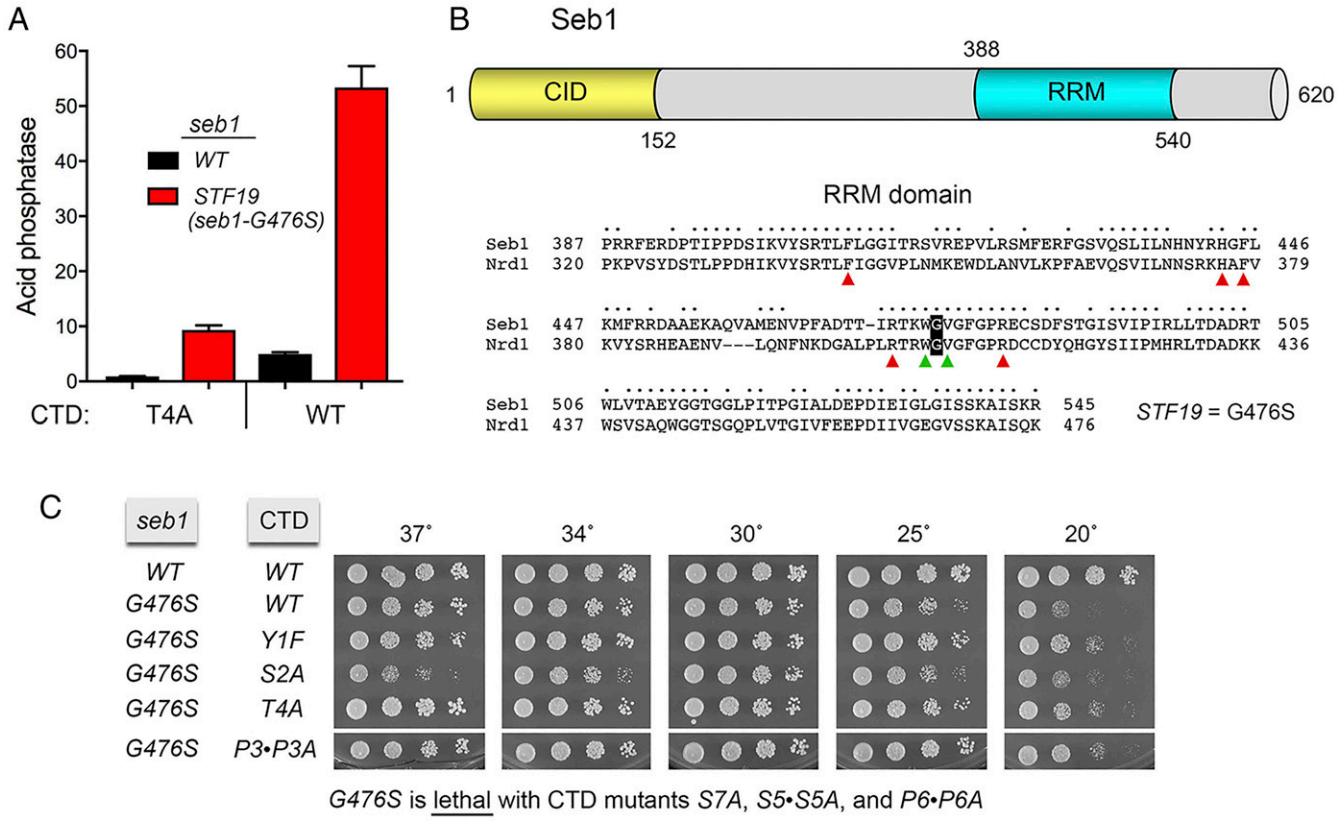

Fig. 1. The *STF* screen identifies an allele of transcription termination factor Seb1. (*A*) *S. pombe* strains bearing the indicated *seb1* and *rpb1-CTD* alleles were grown to A_{600} of 0.5 to 0.8 in liquid culture in YES medium at 30 °C. Cells were then harvested, washed with water, and assayed for Pho1 acid phosphatase activity by conversion of *p*-nitrophenylphosphate to *p*-nitrophenol. Activity is expressed as the ratio of A_{410} (*p*-nitrophenol production) to A_{600} (input cells). Each datum in the bar graph is the average of assays using cells from at least three independent cultures ± SEM. (*B*) Seb1 is composed of an N-terminal CID (colored gold) and an RRM-type RNA-binding domain (colored cyan) flanked by central and carboxyl-terminal segments (gray) that are predicted to be structurally disordered. The amino acids at the termini and the domain boundaries are indicated by number. The amino acid sequence of the Seb1 RRM domain is aligned to that of *Saccharomyces cerevisiae* Nrd1. Positions of side chain identity/similarity are denoted by dots above the alignment. The conserved Gly476 that was mutated to serine in the *STF19* strain is highlighted in white font on a black background. Conserved amino acids that make atomic contact with RNA in Nrd1•RNA crystal structures are denoted by arrowheads: red for side chain contacts and green for main chain contacts. (*C*) *S. pombe* strains with genotypes as specified on the left were grown in liquid culture at 30 °C. Serial fivefold dilutions were spotted to YES agar and incubated at the indicated temperatures. As noted below the panels, *seb1-G476S* was lethal in combination with CTD alleles *S7A*, *S5•S5A*, and *P6•P6A*.

viable in combination with mutations in CPF and Rhn1, in which context Pho1 was also derepressed (22). These findings implicated the Asp1 pyrophosphatase in constraining 1,5-IP8 or 1-IP7 synthesis by Asp1 kinase, without which 1-IPPs can accumulate to toxic levels that elicit precocious termination by CPF/Rhn1.

Although the results of the initial *STF* screen strengthened the case for IPPs as agonists of 3′-processing/termination, they did not shed light on non-IPP modulators of lncRNA-dependent transcription interference with the *PHO* regulon. To date, nearly all of the players in the *PHO* transcription interference phenomenon have been identified and characterized based on gene deletions or targeted missense mutations, most of which, perforce, involve inessential components of the 3′-processing/termination pathway(s). Other than Rpb1, we have little appreciation of the contributions of essential transcriptional/processing factors to fission yeast phosphate homeostasis.

Notwithstanding that Asp1 pyrophosphatase mutations dominated the output of the initial *STF* screen, we sought to maximize the utility of the *STF* assay and seek out additional genes that confer the *STF* phenotype by subjecting a larger pool of "*STF* positive" isolates to focused sequencing of their *asp1* genes and excluding any that had acquired *asp1* mutations. In this way, we obtained strain *STF19*, which has a single missense mutation (Gly476Ser) in the RNA-binding domain of the essential termination factor Seb1. The *seb1-G476S* allele derepresses *pho1* (and *tgp1*) in a wild-type CTD background, and this effect is squelched by CPF and Rhn1 mutations and by inactivation of the Asp1 IPP kinase. The genetic and structural evidence reported here suggests that *seb1-G476S* is a heretofore unique gain-of-function mutation of Seb1 with respect to 3′-processing/termination.

Results

The *STF* Screen Identifies an Allele of Transcription Termination Factor Seb1. Testing individual colonies of mutagenized *CTD-T4A* cells for cell surface acid phosphatase activity by a colorimetric colony overlay assay was performed as described previously (22). In our first round of screening, whole-genome sequencing showed that 12/12 independent *STF* strains had Asp1 pyrophosphatase mutations. Analysis of a second set of six independent *STF* isolates by focused PCR amplification of the Asp1 pyrophosphatase open reading frame (ORF) and sequencing the PCR product showed that all of them had Asp1 pyrophosphatase mutations (22). Here, by applying the *asp1* gene sequencing as a pretest for new candidate *STF* isolates, we identified an *STF* strain that had a wild-type *asp1*$^{+}$ locus. This strain was backcrossed twice to a *T4A* strain of the opposite mating type and subjected to random spore analysis, whereby populations of haploid progeny (250 to 400) were tested for Pho1 acid phosphatase activity via the overlay assay. In both backcrosses, ∼50% of the haploid progeny stained red and ∼50% were pale, signifying that the *STF* phenotype results from a mutation in a single gene. The *T4A* strain bearing this *STF* allele, provisionally named *STF19*, and the parental *T4A* strain were assayed quantitatively for Pho1 activity after growth at 30 °C in phosphate-replete liquid medium. *STF19 T4A* cells expressed 11-fold higher acid phosphatase activity than the *T4A* parent (Fig. 1*A*). *STF19 T4A* cells grew as well as the *T4A* parent on YES agar at all temperatures tested (shown in Fig. 1*C* and *SI Appendix*, Fig. S4, respectively).

Paired-end Illumina sequencing of unamplified genomic DNA from the *STF19* strain was performed as described (22) to achieve at least 100-fold coverage of the yeast genome. Compared to the genome of the parental *T4A* strain, the *STF19* strain had acquired a missense mutation—Gly476Ser—in the gene encoding the essential transcription termination factor Seb1.

The G476S Mutation in Seb1. Seb1 was originally identified in a yeast two-hybrid screen for proteins that interact with the Rpb7 subunit of fission yeast Pol2 (26). It was recognized as a homolog of the budding yeast RNA-binding protein Nrd1 and was shown to be essential for vegetative growth of fission yeast (26). The 620-aa Seb1 protein consists of a CTD interaction domain (CID; amino acids 1 to 152) and an RNA recognition module (RRM) RNA-binding domain (amino acids 388 to 540) (Fig. 1*B*), the structures of which have been determined (21). The central and carboxyl-terminal segments of Seb1 are predicted to be structurally disordered. The CID and RRM domain are both required for cell viability (21). The CID binds in vitro to a Ser2 phosphorylated di-heptad CTD repeat peptide with threefold higher affinity versus a Ser5 phosphorylated CTD peptide, 10-fold higher affinity versus a Ser7 phosphorylated CTD, and >40-fold higher affinity compared to an unphosphorylated CTD peptide (21). Affinity for the Thr4 phosphorylated CTD ligand was within a factor of two of that for the Ser2-PO_4 CTD, while binding to a Tyr1-PO_4 CTD peptide was similar to the unphosphorylated CTD (27). The evidence that Seb1 is an agent of 3′-processing/termination is compelling. To wit: 1) Seb1 is physically associated in vivo with the CPF complex, Rhn1, and the torpedo 5′ exoribonuclease Dhp1; 2) Seb1 is present and enriched at the 3′ end of Pol2 transcription units; 3) depletion of Seb1 or replacement of depleted Seb1 with a quadruple-alanine mutant in the RRM domain (R442A-H443A-F445A-K447A) results in Pol2 transcription read-through (RT) past normal termination sites; and 4) Seb1 depletion or substitution with the 4xAla RRM mutation favors utilization of distal poly(A) sites (21, 28).

The salient finding here is that the *STF19* mutation G476S maps to the RRM domain of Seb1 (Fig. 1*B*). Genome-wide in vivo protein–RNA cross-linking methods have established that Seb1 recognizes a 5′-GUA trinucleotide sequence motif situated 50 to 100 nt downstream of nascent RNA cleavage/poly(A) sites (21, 28). The Seb1 RNA recognition element resembles the 5′-GUA(A/G) motif recognized by budding yeast Nrd1 (29). A primary structure alignment of the Seb1 and Nrd1 RRM domains highlights 105 positions of side chain identity/similarity (Fig. 1*B*). Crystal structures have been determined for the Seb1 RRM in the absence of RNA and for the Nrd1 RRM in complexes with GUA-containing RNA ligands (21, 29). The five amino acid side chains of Nrd1 RRM that make atomic contacts with the RNA (indicated by red arrowheads in Fig. 1*B*) are conserved perfectly in the Seb1 RRM (as Phe409, His443, Phe445, Arg472, and Arg482). Two Nrd1 amino acids within a conserved Trp-Gly-Val peptide that receive hydrogen bonds to their main chain carbonyls from the uracil-N3 (to Trp) and the adenine-N6 (to Val) of the GUA RNA element are denoted by green arrowheads in Fig. 1*B*. The Gly476 position that is mutated in *STF19* is located within this Trp-Gly-Val motif of the RRM•RNA interface.

Structure of the Mutant Seb1-G476S RRM Domain. Here, we produced, purified, and crystallized the RRM domain of the Seb1-G476S protein. The structure was solved at 1.4-Å resolution and refined to R/R_{free} of 17.1/18.8 (*SI Appendix*, Table S1). The Ser476 RRM domain structure is tightly superimposable on that of the wild-type Seb1 RRM, except that the Ser476 mutation elicits a 2.0- to 2.5-Å shift in the position of the 11-aa loop from Val477 to Ser485 (Fig. 2*A*). Attempts to cocrystallize the Seb1-G476S RRM in complex with a variety of RNA oligonucleotides containing a 5′-GUA triplet were uniformly unsuccessful. Broad crystal screens starting with a mixture of RNA and RNA ligand were undertaken, and multiple conditions were identified that did yield high-resolution diffracting crystals. However, in every case, they turned out to be in the same space group and lattice as the unliganded RRM crystals, and they were devoid of bound RNA. Inspection of these crystal lattices and superposition of the RNA-bound structure of the homologous Nrd1 RRM revealed that the tight contacts between Seb1 RRM and two symmetry-related Seb1 RRM protomers (mediated by many interprotomer pairwise side-chain hydrogen bonds and salt bridges involving

GENETICS

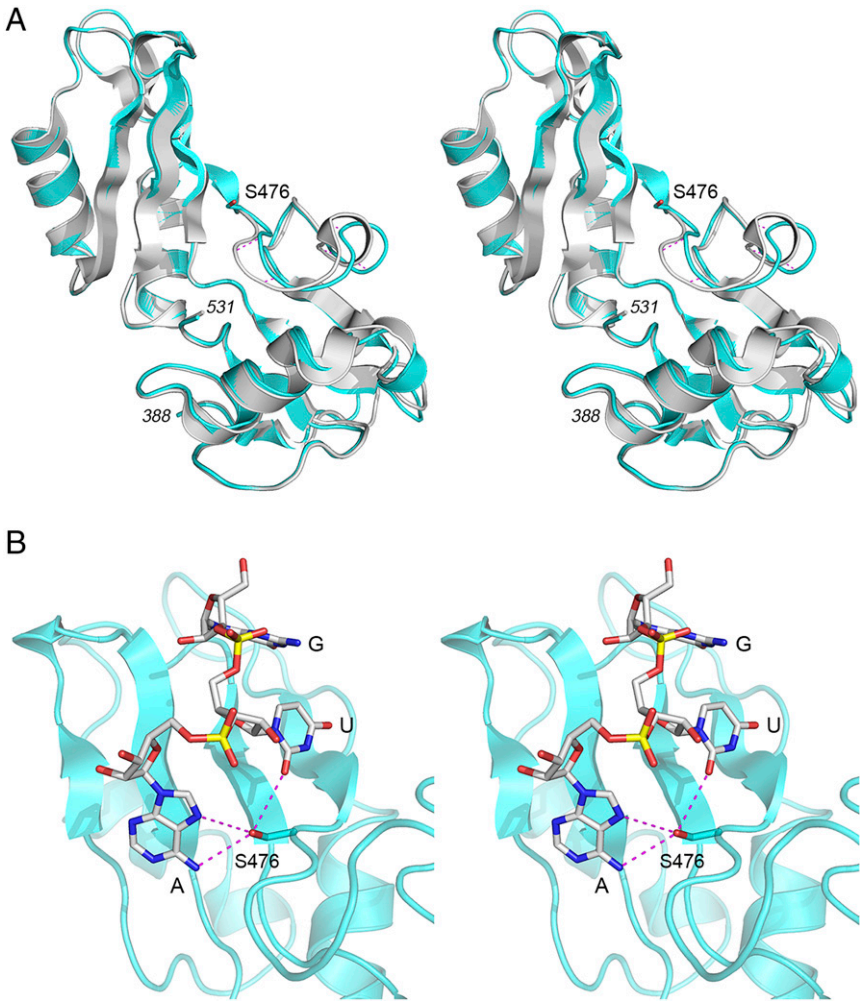

Fig. 2. Structure of the G476S mutant version of the Seb1 RRM domain. (*A*) Stereo view of the tertiary structure of the G476S mutant RRM domain (colored cyan) superimposed on that of the wild-type RRM (colored gray; from Protein Data Bank [PDB] 5MDU). Mutated amino acid Ser476 is shown as a side chain stick model. The mutation elicits a 2.0- to 2.5-Å shift in the position of the 11-aa loop from Val477 to Ser485. Selected C-α atoms in the dislocated loop are connected by magenta dashed lines. (*B*) Stereo view of a model of Seb1-G476S RRM with a 5′-GUA ligand in the RNA-binding site. The 5′-GUA ligand (stick model with gray carbons) is from the homologous Nrd1 RRM•RNA complex structure (PDB 5O1Z) that had been superimposed on the Seb1 RRM. The putative atomic contacts of Ser476-Oγ to uracil-O2 (3.7 Å), adenine-N6 (3.7 Å), and adenine-N7 (3.9 Å) are denoted by magenta dashed lines.

Arg482-Thr509, Arg472-Asp501, Arg415-Glu455, Asn440-Glu455, and Tyr441-Lys402) would definitely occlude the RNA-binding site in Seb1 RRM. Nonetheless, some insight into the consequences of the G476S mutation could be gleaned by importing the 5′-GUA ligand from the superimposed Nrd1•RNA structure into the structure of the Seb1-G476S RRM, which suggests that the installation of Ser476 establishes new atomic contacts of Ser476-Oγ to uracil-O2 (3.7 Å), adenine-N6 (3.7 Å), and adenine-N7 (3.9 Å) moieties of the RNA ligand (Fig. 2*B*).

Effect of the *seb1-G476S* Mutation in a Wild-Type *rpb1-CTD* Background. We crossed the *seb1-G476S T4A* strain, in which the *rpb1-CTD-T4A* locus was flanked by a downstream nourseothricin-resistance marker, with a wild-type *rpb1-CTD* strain in which the *rpb1*$^+$ allele was flanked by a G418-resistance marker. The G418/nourseothricin-resistant diploids were sporulated, and random populations of >1,000 haploid progeny were selected for the resistance markers linked to the *rpb1-CTD-WT* and *rpb1-CTD-T4A* alleles. Populations of *CTD-WT* cells were screened for Pho1 expression by agar overlay, with deep red color indicating presence of the *seb1-G476S* mutation. About half of the *CTD-WT* progeny backcrosses were lightly stained red (i.e., reflecting the fact that the basal level of "repressed" Pho1 activity in *CTD-WT* cells is several-fold higher than the hyperrepressed Pho1 state in *T4A* cells; Fig. 1*A*), and half were darker red. Sequencing of the *seb1* locus in individual darker red *CTD-WT* haploids affirmed the presence of the *seb1-G476S* mutation. Note that the *seb1-G476S* allele per se conferred a slow growth phenotype at low temperatures vis-à-vis the wild-type strain, as gauged by colony size (Fig. 1*C*).

The *seb1-G476S CTD-WT* and *seb1*$^+$ *CTD-WT* strains were grown in phosphate-replete medium at 30 °C and assayed for Pho1 acid phosphatase activity. The *seb1-G476S* allele increased Pho1 expression by 11-fold vis-à-vis the *seb1*$^+$ *CTD-WT* control (Fig. 1*A*). Pho1 expression in *seb1-G476S* cells was sixfold higher in the *CTD-WT* background than in the *CTD-T4A* background, in keeping with the sixfold differential between the basal Pho1 activity in *seb1*$^+$ *CTD-WT* versus *seb1*$^+$ *CTD-T4A* cells (Fig. 1*A*).

To profile the effects of the *seb1-G476S* mutation on the fission yeast transcriptome, we performed RNA sequencing (RNA-seq) on poly(A)$^+$ RNA isolated from *seb1-G476S* cells and a wild-type *seb1*$^+$ control strain, both of which were wild-type with respect to the Pol2 CTD. Complementary DNAs obtained from three biological replicates (using RNA from cells grown to midlog phase in YES medium at 30 °C) were sequenced

for each strain. In the datasets, 95 to 97% of the reads were mapped to *Schizosaccharomyces pombe* genomic loci (*SI Appendix*, Table S2). Read densities for individual genes were highly reproducible between biological replicates (Pearson coefficients of 0.98 to 0.99) (*SI Appendix*, Table S3). A cutoff of ±2-fold change in normalized transcript read level and an adjusted *P* value of ≤0.05 were the criteria applied to derive an initial list of differentially expressed annotated loci. We then focused on differentially expressed genes with average normalized read counts ≥100 in either the *seb1-G476S* or *seb1*$^{+}$ strains in order to eliminate transcripts that were expressed at very low levels in vegetative cells. We thereby identified sets of 107 and 97 annotated protein-coding genes that were respectively up-regulated and down-regulated by these criteria in *seb1-G476S* cells. The up-regulated gene set included *tgp1* (up ninefold) and *pho1* (up fourfold). RNA-seq revealed no increase in *seb1-G476S* cells of the mRNA encoding Pho7, the transcription factor that drives *pho1* and *tgp1* mRNA synthesis.

***seb1-G476S* Genetic Interactions with CTD Mutations.** We crossed the *seb1-G476S CTD-WT* strain with strains bearing differentially marked *rpb1-CTD* alleles lacking the three other inessential CTD phospho-sites: *Y1F*, in which Tyr1 in all heptad repeats was replaced by Phe; *S2A*, in which all Ser2 positions were changed to Ala; and *S7A*, in which all Ser7 residues were replaced by Ala. Whereas the *Y1F* and *S2A* mutations do not affect Pho1 expression, the *S7A* allele results in Pho1 derepression dependent on CPF and Rhn1 (12). We also crossed *seb1-G476S* to strains with chimeric mutations of the three essential letters of the CTD code: the *P3•P3A*, *S5•S5A*, and *P6•P6A* mutant CTDs in which Pro3, Ser5, or Pro6 in every other repeat was replaced by alanine. The *S5•S5A*, and *P6•P6A* alleles derepress Pho1 under phosphate-replete conditions (13, 30). Random populations of haploid progeny were selected for the mutant *CTD* allele, assayed for Pho1 activity, and screened for the *seb1-G476S* mutation by sequencing of the *seb1* locus (as described in *SI Appendix, Methods*). We readily obtained *seb1-G476S CTD-Y1F*, *seb1-G476S CTD-S2A*, and *seb1-G476S CTD-P3•P3A* double mutants at the expected frequency, and they grew well on YES agar at 30 °C (Fig. 1*C*). The *seb1-G476S CTD-S2A* strain displayed a slow growth defect at 37 °C, as seen previously for the *CTD-S2A* single mutant (12). By contrast, we did not recover any viable double mutants of *seb1-G476S* with *CTD* alleles *S7A*, *S5•S5A*, or *P6•P6A*.

To verify this result, we replaced the *seb1* locus in a wild-type strain with *seb1*$^{+}$ or *seb1-G476S* alleles marked with a 3′ flanking *hygMX* drug resistance cassette, which enabled us to screen a large population of random spores from the pairwise mating of *seb1-G476S* to the *CTD-S7A*, *S5•S5A*, and *P6•P6A* strains. Failure to recover any viable double mutants signified that the *seb1-G476S* mutation is synthetically lethal with CTD mutations *S7A*, *S5•S5A*, and *P6•P6A*.

Derepression of *pho1* Expression by *seb1-G476S* Depends on CPF Subunits and Rhn1. To test the idea that *seb1-G476S* elicits a gain of Seb1 function that leads to precocious termination during *prt* lncRNA synthesis, we performed pairwise mating of *seb1-G476S* cells with knockout strains lacking the Dis2, Ctf1, Ppn1, or Swd22 subunits of the CPF complex, a strain with a catalytically dead (C13S) version of the Ssu72 protein phosphatase subunit of CPF, and a strain that lacks the transcription termination factor Rhn1. Viable double-mutant haploids were recovered after sporulation of the diploids in each case. Spot tests of the double mutants and parental single mutants for growth on YES agar are shown in Fig. 3*A*. *seb1-G476S* displayed no synthetic growth defects with *ctf1*Δ or *dis2*Δ. Notable findings were that *seb1-G476S* rescued the *ts* growth defect of *rhn1*Δ at 37 °C, while *rhn1*Δ rescued the *cs* growth defect of *seb1-G476S* at 20 °C (Fig. 3*A*), consistent with a yin-yang relationship between gain and loss of termination function in the *seb1-G476S* and *rhn1*Δ genetic backgrounds. *seb1-G476S* also improved the growth of *ssu72-C13S* cells at 37 °C (Fig. 3*A*). The *cs* phenotype of *seb1-G476S* was exacerbated at 25 °C by *ppn1*Δ and *swd22*Δ.

The single and double mutants were assayed for acid phosphatase activity during growth in phosphate-replete medium at 30 °C. The instructive findings were that the derepression of Pho1 by *seb1-G476S* was effaced in *ppn1*Δ, *swd22*Δ, and *rhn1*Δ cells and was severely attenuated in *ssu72-C13S*, *ctf1*Δ, and *dis2*Δ cells (Fig. 3*B*). Thus, the increase in Pho1 expression in *seb1-G476S* cells requires CPF subunits and Rhn1, consistent with the Seb1 gain-of-function hypothesis.

Derepression of *pho1* and *tgp1* by *seb1-G476S* Depends on Upstream lncRNA Poly(A) Signals. Plasmid-based reporter systems have been developed that recapitulate the salient features of lncRNA-mediated transcriptional interference with the *pho1* and *tgp1* promoters (10, 11). The *prt–pho1* reporter cassette contains the tandem *prt* and *pho1* genes spanning from 1,831 nucleotides upstream of the *pho1* ORF (comprising the *prt* promoter and *prt* lncRNA) to 647 nucleotides downstream of the *pho1* ORF (Fig. 4*A*). The *prt* transcription start site is located 1,147 nucleotides upstream of the *pho1* transcription start site. The *prt* lncRNA that interferes with *pho1* expression is a long RT transcript that initiates from the *prt* promoter, traverses the Pho7 transcription factor binding sites in the *pho1* mRNA promoter, and terminates at the *pho1* mRNA poly(A) site (Fig. 4*A*). There are two classes of short *prt* lncRNAs (Fig. 4*A*) that are cleaved and polyadenylated at sites +351 and +589 in response to two different upstream poly(A) signals (PAS). Enhancement of nascent RNA processing via the short *prt* lncRNA PAS elements will terminate Pol2 transcription upstream of the Pho7 binding sites in the *pho1* mRNA promoter and thus alleviate transcription interference. Conversely, simultaneous nucleobase substitution mutations of the two short *prt* PAS elements of the *prt–pho1* reporter results in hyperrepression of the flanking *pho1* promoter (12). Here, we deployed the reporter system to interrogate the role of *prt* lncRNA 3′-cleavage/polyadenylation in *pho1* derepression by *seb1-G476S*. *prt–pho1* plasmids with wild-type or mutant PAS elements were introduced into [*prt2-pho84-prt-pho1*]Δ cells bearing *WT* or *G476S seb1* alleles. Transformants were assayed for acid phosphatase activity during growth in phosphate-replete medium. Pho1 expression from the wild-type plasmid was increased sevenfold in *seb1-G476S* cells versus *seb1-WT* cells (Fig. 4*B*), thereby echoing the derepressive effect of *seb1-G476S* on *pho1* expression from the chromosomal *prt–pho1* locus. The crucial finding was that the derepressed level of Pho1 expression in *seb1-G476S* cells was strongly attenuated (10-fold) by dual PAS mutations that interdict precocious *prt* lncRNA 3′-processing at the two promoter-proximal sites.

The *nc-tgp1–tgp1* reporter cassette (*nc-tgp1–tgp1*$_{prom}$*·pho1*) includes a fragment of the *nc-tgp1–tgp1* locus, spanning 301 nucleotides upstream of the *nc-tgp1* transcription initiation site (encompassing the putative *nc-tgp1* promoter) and the entire 1,865-nt segment between the *nc-tgp1* transcription start site and the *tgp1* translation start codon (containing the *tgp1* promoter and *tgp1* transcription start site) fused to the *pho1* ORF and its native 3′ flanking DNA (Fig. 4*C*). The *nc-tgp1* transcription start site is located 1,823 nt upstream of the *tgp1* transcription start site. The *nc-tgp1* transcript that interferes with *tgp1* expression is cleaved and polyadenylated at nucleotide +1636 of the *nc-tgp1* transcription unit, which is located within the DNA-binding site for Pho7, the transcription factor that drives *tgp1* expression (11). A short form of the *nc-tgp1* lncRNA is cleaved/polyadenylated at position +504 of the *nc-tgp1* transcription unit, which is 17 nt downstream of a consensus fission yeast PAS. Mutation of the PAS for the short *nc-tgp1* lncRNA in the *nc-tgp1–tgp1* reporter

GENETICS

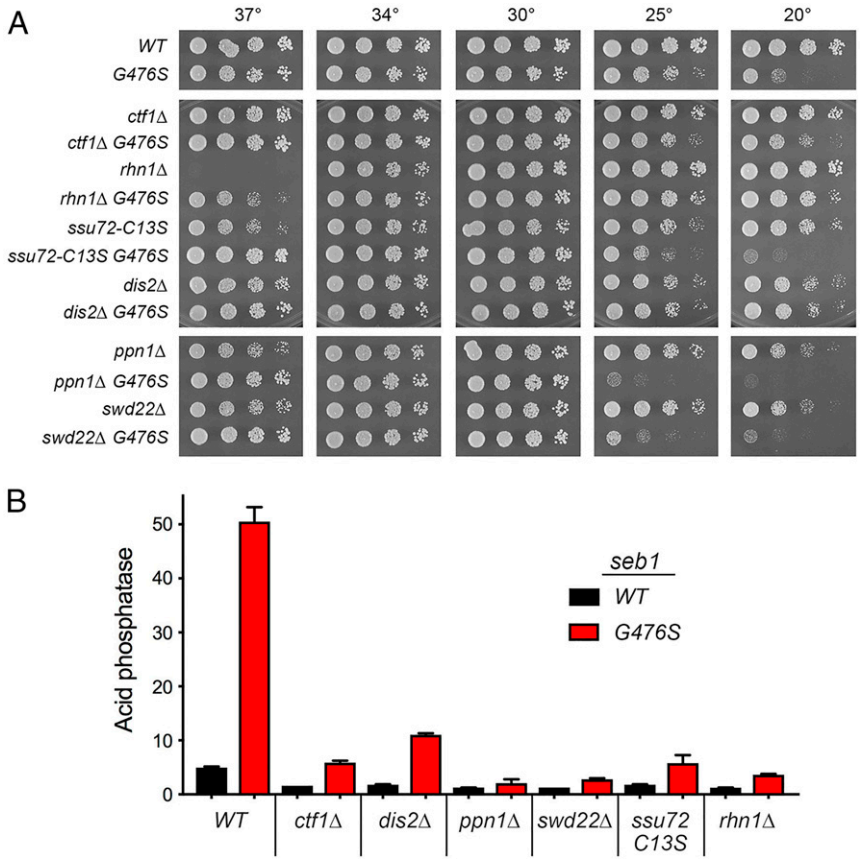

Fig. 3. Derepression of *pho1* expression by *seb1-G476S* depends on CPF subunits and Rhn1. (*A*) *S. pombe* strains with genotypes as specified on the left were spot tested for growth on YES agar at the indicated temperatures. (*B*) Strains bearing the indicated *seb1* alleles (wild-type or *G476S*) in combination with CPF subunit or Rhn1 mutations as specified were grown in liquid culture at 30 °C and assayed for acid phosphatase activity.

abolished derepression of the downstream *tgp1* mRNA promoter in a *CTD-S5A* strain background (11). Here, we found that *tgp1* promoter–driven acid phosphatase expression was increased 30-fold in *seb1-G476S* cells versus *seb1-WT* cells and that this derepression was effaced by mutating the promoter-proximal *nc-tgp1* PAS (Fig. 4*D*).

RNA Analysis Confirms that *seb1-G476S* Elicits Precocious lncRNA Termination. We performed Northern blot analysis of RNAs isolated from three independent cultures of *seb1-WT* and *seb1-G476S* cells bearing the *nc-tgp1–tgp1* reporter plasmid (Fig. 4*E*). Probing the blot with a radiolabeled oligonucleotide complementary to the 5′ end of the *nc-tgp1* transcript, we found that the steady-state level of the *nc-tgp1-short* lncRNA was increased markedly in *seb1-G476S* cells vis-à-vis the wild-type controls (Fig. 4*E*). We conclude that the *G476S* mutation enhanced utilization of the 5′-proximal poly(A) site and thus precocious termination of *nc-tgp1* lncRNA transcription, thereby accounting for increased expression of the downstream flanking mRNA. We also conducted Northern analysis of the *prt* transcript from three independent cultures of *seb1-WT* and *seb1-G476S* cells bearing the *prt–pho1* reporter (Fig. 5). A 5′ *prt* probe detected the interfering *prt-pho1* RT transcript as the major lncRNA species in wild-type cells (Fig. 5*B*). Formation of the *prt-pho1* RT transcript was almost completely squelched in *seb1-G476S* cells. Yet it was not the case that the decrement in the long *prt-pho1* RT transcript in *seb1-G476S* cells was accompanied by an increase in the steady-state levels of the short *prt* PAS and *prt* PAS2 RNAs. *prt* transcripts can be challenging to detect because they are turned over rapidly via the two clusters of DSR (determinant of selective removal) elements encoded within the proximal segment of the transcript (the DSRs are denoted by the blue boxes in the cartoon diagram in Fig. 5*A*) (10). Therefore, we tested a version of the *prt–pho1* reporter in which the consensus DSR sequences in the two DSR clusters are altered by base substitutions (10). A *prt*-probed Northern blot of RNAs isolated from two independent cultures of *seb1-WT* and *seb1-G476S* cells bearing the mutated DSR *prt–pho1* reporter revealed that the *seb1-G476S* allele strongly skewed the distribution of *prt* lncRNAs toward production of the precociously terminated *prt* PAS2 species, at the expense of the *prt-pho1* RT transcript (Fig. 5*B*). Quantification of the signal intensity of these two *prt* transcripts yielded PAS2 to RT ratios of 0.16 and 0.17 for two RNA samples from *seb1-WT* cells and 1.49 and 1.64 for the RNAs from *seb1-G476S* cells (i.e., there was an average 9.5-fold increase in apparent precocious termination directed by PAS2).

The results of the experiments in Figs. 3–5 collectively fortify the case for *seb1-G476S* as a gain-of-function mutation in Seb1 that elicits precocious lncRNA termination dependent on lncRNA PAS and cleavage/polyadenylation factors.

Interface of *seb1-G476S* and Inositol Pyrophosphate Metabolism. Previous studies showed that derepression of Pho1 elicited by the Pol2 *CTD-S7A* mutation or a deletion of Erh1 depends on the activity of the IPP kinase Asp1 (14, 25). Asp1 is a bifunctional enzyme composed of an N-terminal IPP kinase domain that converts 5-IP7 to 1,5-IP8 and a carboxyl-terminal IPP pyrophosphatase domain that converts 1,5-IP8 back to 5-IP7 (23, 24) (Fig. 6*C*). The

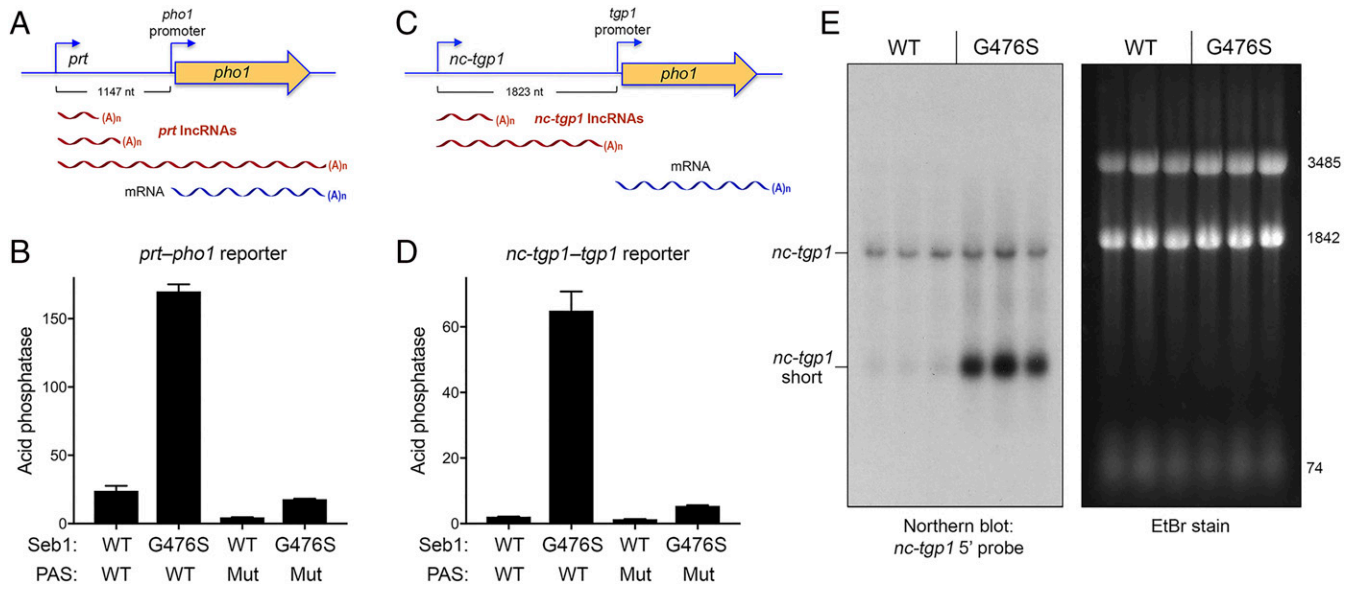

Fig. 4. Derepression of *pho1* and *tgp1* by *seb1-G476S* depends on upstream lncRNA PASs. (*A*) Schematic of the *prt–pho1* locus in the reporter plasmid. Transcription start sites are indicated by bent blue arrows with the intervening distance indicated by the bracket. The *prt* lncRNAs are depicted as red wavy lines. The *pho1* mRNA is a blue wavy line. (*B*) *prt–pho1* reporter plasmids with wild-type (WT) or mutated (Mut) *prt* 5′-proximal polyadenylation signals PAS and PAS2 were transfected into *seb1-WT pho1*Δ or *seb1-G476S pho1*Δ cells. Plasmid-bearing cells were grown in liquid culture at 30 °C and assayed for acid phosphatase activity. (*C*) Schematic of the *nc-tgp1–tgp1(promoter)•pho1* locus in the reporter plasmid. Transcription start sites are indicated by bent blue arrows with the intervening distance indicated by the bracket. The *nc-tgp1* lncRNAs are depicted as red wavy lines. The *tgp1* promoter–driven mRNA is a blue wavy line. (*D*) *nc-tgp1–tgp1(promoter)•pho1* reporter plasmids with a WT or Mut *nc-tgp1* 5′-proximal polyadenylation signal were transfected into *seb1-WT pho1*Δ or *seb1-G476S pho1*Δ cells. Plasmid-bearing cells were grown in liquid culture at 30 °C and assayed for acid phosphatase activity. (*E*) Northern blot analysis of *nc-tgp1* RNA. RNA was isolated from three independent cultures of *seb1-WT pho1*Δ or *seb1-G476S pho1*Δ cells bearing the wild-type *nc-tgp1–tgp1(promoter)•pho1* reporter plasmid. The RNAs were resolved by formaldehyde agarose gel electrophoresis. The gel was stained with ethidium bromide (shown in right panel, with sizes of the stained ribosomal RNAs and transfer RNAs indicated in nucleotides) prior to transferring the resolved RNAs to a membrane, which was then hybridized to a ^{32}P-labeled probe complementary to *nc-tgp1* nucleotides 70 to 108. An autoradiograph of the Northern blot is shown in the left panel. The species corresponding to *nc-tgp1* short and full-length *nc-tgp1* lncRNA are indicated.

in vivo effect of an *asp1*Δ null allele or a kinase-dead *asp1-D333A* allele is to eliminate intracellular IP8 and 1-IP7 and to increase the level of 5-IP7 (23). To see if IPP status affects Pho1 derepression by the Seb1-G476S mutation, we crossed *hygMX*-marked *seb1-G476S* to *asp1*Δ and *asp1-D333A* strains. *asp1*Δ and *asp1-D333A* cells themselves display a *cs* growth phenotype (25). Here, we recovered viable *seb1-G476S asp1*Δ and *seb1-G476S asp1-D333A* haploid progeny that grew more slowly than wild-type at 30 °C (as gauged by colony size) but were very sick at 25 °C and 20 °C and failed to grow at 37 °C (Fig. 6*A*). Assays of cell surface acid phosphatase activity of cells grown at 30 °C showed that the derepression of Pho1 activity by *seb1-G476S* was erased in the *asp1*Δ and *asp1-D333A* backgrounds (Fig. 6*B*), signifying a requirement for 1-IPP synthesis and an agonist role for 1-IPPs in Seb1-mediated 3′-processing/termination during *prt* transcription.

The fission yeast proteome includes two IPP pyrophosphatase enzymes that convert IP8 to IP7 and have demonstrated roles in repression of the *PHO* genes in a manner dependent on CPF and Rhn1 (25). The carboxyl-terminal IPP pyrophosphatase domain of Asp1, which belongs to the histidine acid phosphatase family, hydrolyzes the 1-pyrophosphate of IP8 to generate 5-IP7 (23, 24) (Fig. 6*C*). Aps1, a Nudix family enzyme, acts on the 5-pyrophosphate of IP8 to generate 1-IP7 (31, 32) (Fig. 6*C*). Neither pyrophosphatase activity is essential per se for fission yeast vegetative growth, i.e., the pyrophosphatase-defective *asp1-H397A* strain and the *aps1*Δ null strain grow well on YES agar at 20 to 37 °C (25). We queried epistasis of *seb1-G476S* with the two IPP pyrophosphatases with respect to cell growth and Pho1 expression by attempting to construct *seb1-G476S asp1-H397A* and *seb1-G476S aps1*Δ double-mutant strains via mating and sporulation. We recovered (by random spore analysis) *seb1-G476S asp1-H397A* progeny that grew very poorly on YES agar at all temperatures tested (Fig. 6*A*). The *seb1-G476S* and *aps1*Δ alleles were synthetically lethal; to wit: 1) we were unable to obtain viable double mutants after screening a large population of haploid progeny of the genetic cross; and 2) wild-type progeny and the differentially marked *seb1-G476S* and *aps1*Δ single mutants were recovered at the expected frequencies. Although *seb1-G476S asp1-H397A* cells grew slowly in liquid medium at 30 °C, an assay of acid phosphatase showed that the double mutant expressed threefold higher levels of Pho1 than the *seb1-G476S* single mutant (Fig. 6*B*). Pho1 expression in *seb1-G476S asp1-H397A* cells was ∼70% higher than that in the *asp1-H397A* single mutant (25), indicative of an additive effect of the Seb1-G476S and Asp1 pyrophosphatase-dead mutations on *pho1* derepression.

A comparison of the presently reported RNA-seq data for *seb1-G476S* to the transcriptome profiles of the *aps1*Δ and *asp1-H397A* strains reported previously (25) revealed eight protein-coding RNAs that were coordinately up-regulated by >2-fold in all three genetic backgrounds (*SI Appendix*, Fig. S1). This set included the following: the *PHO* genes *tgp1* and *pho1*; *ecl3* (located adjacent to the *pho84–pho1* gene cluster and coregulated with the *PHO* genes; 13, 22, 30); the putative phosphate acquisition gene *SPAC1039.02* (encoding an extracellular 5′-nucleotidase); *mbx2* (a gene likely to be subject to flanking lncRNA-mediated transcriptional interference; 25); the uracil-regulatable genes *urg1* and *urg2*; and *SPBC25B2.08* encoding a predicted polypeptide unique to *S. pombe*.

Rescue of *seb1-G476S* Synthetic Lethality by CPF/Rhn1 Mutations. In light of the findings that the *seb1-G476S* mutation, which

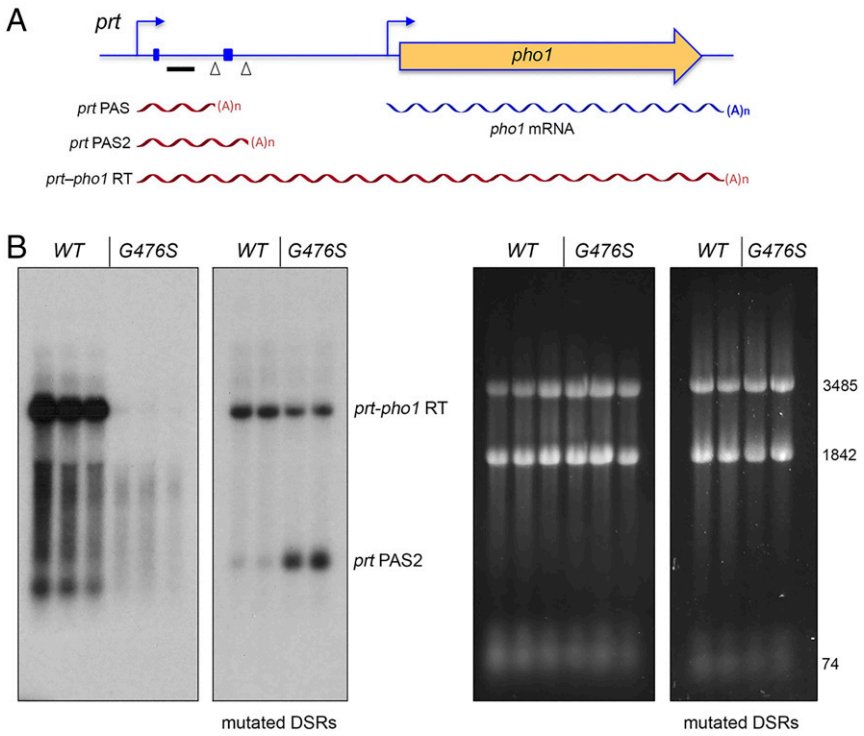

Fig. 5. *seb1-G476S* elicits precocious *prt* lncRNA termination. (*A*) Schematic of the *prt–pho1* locus in the reporter plasmid. Transcription start sites are indicated by bent blue arrows. Two DSR element clusters in the *prt* transcription unit are denoted by small blue boxes. The 5′-proximal PAS and PAS2 polyadenylation signals are denoted by triangles. The *prt* lncRNAs are depicted as red wavy lines. A ^{32}P-labeled probe complementary to *prt* nucleotides 160 to 202 is denoted by a black bar. The *pho1* mRNA is a blue wavy line. (*B*) Northern blot analyses of *prt* lncRNA. RNA was isolated from three independent cultures of *seb1-WT pho1*Δ and *seb1-G476S pho1*Δ cells bearing the wild-type *prt–pho1* reporter plasmid or from two independent cultures of *seb1-WT pho1*Δ and *seb1-G476S pho1*Δ cells bearing a *prt–pho1* reporter plasmid in which both of the DSR clusters were inactivated by multiple base-substitution mutations. Photographs of the ethidium bromide–stained gels are shown in the right panels. The annealed ^{32}P-labeled *prt* probe was detected by autoradiography of the Northern blot membrane, as shown in the left panels. The species corresponding to *prt* PAS2 and *prt–pho1* RT lncRNAs are indicated.

derepresses *pho1*, was inviable in combination with several other mutations that derepress *pho1*, we queried whether such synthetic lethality could be suppressed by mutations in the 3′-processing/termination machinery (i.e., CPF subunits and Rhn1). Specifically, we performed pairwise crosses of *seb1-G476S* and double mutants *aps1*Δ *ctf1*Δ, *aps1*Δ *ssu72-C13S*, *aps1*Δ *rhn1*Δ, *CTD-S7A ctf1*Δ, or *CTD-S7A ssu72-C13S* and screened haploid progeny for the drug-resistance markers linked to the *seb1-G476S*, *aps1*Δ, *CTD-S7A*, and *CPF/rhn1* loci. We thereby recovered the following viable triple mutants: *seb1-G476S aps1*Δ *ctf1*Δ, *seb1-G476S aps1*Δ *ssu72-C13S*, *seb1-G476S aps1*Δ *rhn1*Δ, *seb1-G476S CTD-S7A ctf1*Δ, and *seb1-G476S CTD-S7A ssu72-C13S*. The triple mutants were spot tested for growth on YES agar (Fig. 7*A*). The otherwise lethal *seb1-G476S aps1*Δ combination ameliorated the *ts* growth defect of *rhn1*Δ at 37 °C while conferring a strong *cs* phenotype at 20 and 25 °C (Fig. 7*A*). Rescue of the synthetic lethality of *seb1-G476S aps1*Δ and *seb1-G476S CTD-S7A* by CPF or Rhn1 loss-of-function mutations leads us to conclude that the synthetic lethality is a consequence of overzealous precocious termination of transcription of one or more fission genes that are essential for vegetative growth. The rescued triple mutants were assayed for Pho1 expression during growth in phosphate-replete medium (Fig. 7*B*). The level of Pho1 activity was higher in the *seb1-G476S aps1*Δ *ctf1*Δ cells than in either the *seb1-G476S* or *aps1*Δ single mutants. *seb1-G476S aps1*Δ *ssu72-C13S* and *seb1-G476S aps1*Δ *rhn1*Δ cells expressed Pho1 at a level slightly lower than the *aps1*Δ single mutant. The *seb1-G476S CTD-S7A ctf1*Δ strain had lower Pho1 activity than the *CTD-S7A* single mutant but still higher than wild-type cells. Pho1 was strongly hyperrepressed in *seb1-G476S CTD-S7A ssu72-C13S* cells to well below the wild-type level (Fig. 7*B*).

***seb1-G476S* Elicits an Upstream Shift in Poly(A) Site Utilization in Certain mRNAs.** To explore the idea that *seb1-G476S* might lead to precocious 3′-processing of fission yeast mRNAs, we mined the pooled RNA-seq data from three biological replicates to identify mRNA poly(A) sites. In brief, the unmapped strand-specific RNA-seq reads were trimmed of 5′-oligo(T) tracts and then remapped to the *S. pombe* genome to reveal narrow peaks of sequence reads with an acute falloff at sites of cleavage and 3′ poly(A) addition. This approach accurately identified the single poly(A) site in the *adh1* gene and the three poly(A) sites in the *act1* gene (*SI Appendix*, Fig. S2) that had been mapped previously by using an RNA-seq method that focused specifically on isolated 3′-terminal fragments of poly(A)$^+$ RNAs (33). The *adh1* and *act1* poly(A) sites were reproducible when comparing the data from the individual biological replicates (*SI Appendix*, Fig. S2). Comparison of the wild-type and *seb1-G476S* datasets highlighted poly(A) sites that were differentially utilized in *seb1-G476S* cells vis-à-vis wild-type cells. These entailed either 1) a switch in poly(A) site preference toward a proximal site within the mRNA transcription unit, manifest as an increased ratio of proximal to distal site utilization; or 2) cleavage at a new upstream poly(A) site in *seb1-G476S* cells that was not detectably utilized in wild-type cells.

For example, two distinct *seb1-G476S*–dependent "neo" poly(A) sites were present in the second intron of the *dbp2* gene that were not evident in wild-type controls (Fig. 8*A*). Because there are very few total RNA-seq reads derived from the second

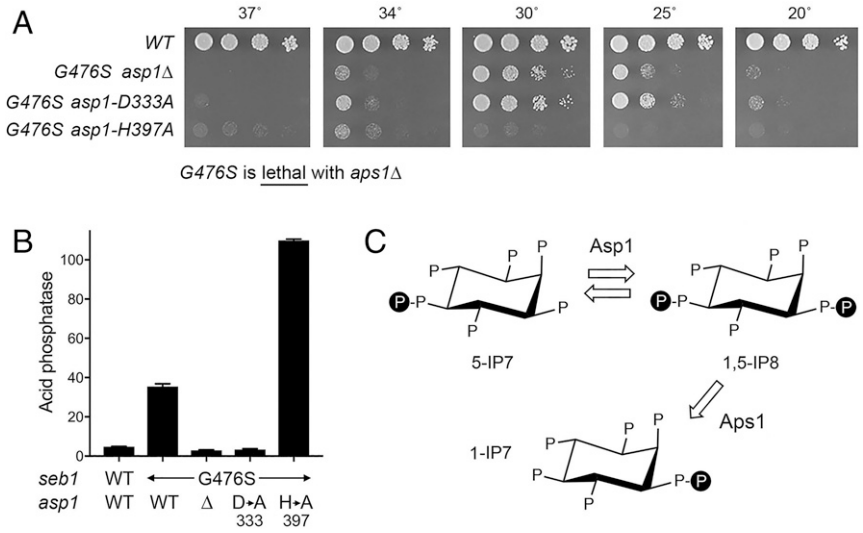

Fig. 6. Interface of *seb1-G476S* and IPP metabolism. (*A*) *seb1*$^{+}$ *asp1*$^{+}$ cells (*WT*) and cells harboring the *seb1-G476S::hygMX* allele in combination with mutants *asp1*Δ, *asp1-D333A* (kinase-defective), or *asp1-H397A* (pyrophosphatase-defective) were spot tested for growth on YES agar at the indicated temperatures. *seb1-G476S* was lethal in the absence the Nudix-family IPP pyrophosphatase enzyme Aps1. (*B*) Strains bearing the indicated *seb1* and *asp1* alleles were grown in liquid culture at 30 °C and assayed for acid phosphatase activity. (*C*) Scheme of IPP metabolism by Asp1 and Aps1. Structures of 5-IP7, 1,5-IP8, and 1-IP7 are shown. Asp1 kinase converts 5-IP7 to IP8, and the Asp1 pyrophosphatase reverses this process. Aps1 pyrophosphatase converts IP8 to 1-IP7.

intron in wild-type cells, the switch to the *dbp2* intronic sites in *seb1-G476S* cells is readily appreciated in the total RNA-seq data, which shows that intronic sequences 3′ of exon 2 and preceding the neo poly(A) sites are present in the precociously terminated *dbp2* transcripts (Fig. 8*A*). Inspection of the poly(A)-adjacent reads in wild-type and *seb1-G476S* cells pinpointed three closely clustered cleavage/polyadenylation sites in the 3′-UTR, preceded by an AAUAAA PAS (Fig. 8 *B*, *Top*). By contrast, the intronic neo poly(A) sites utilized in *seb1-G476S* cells are not preceded by any of the hexanucleotide PASs that have been reported in fission yeast (33, 34). Whereas five GUA Seb1 RNA-binding motifs are located within the 80-nt region downstream of the poly(A) site cluster in the 3′-UTR, only two GUA sites are located in the 85-nt region downstream of the second intronic neo poly(A) site (Fig. 8*B*).

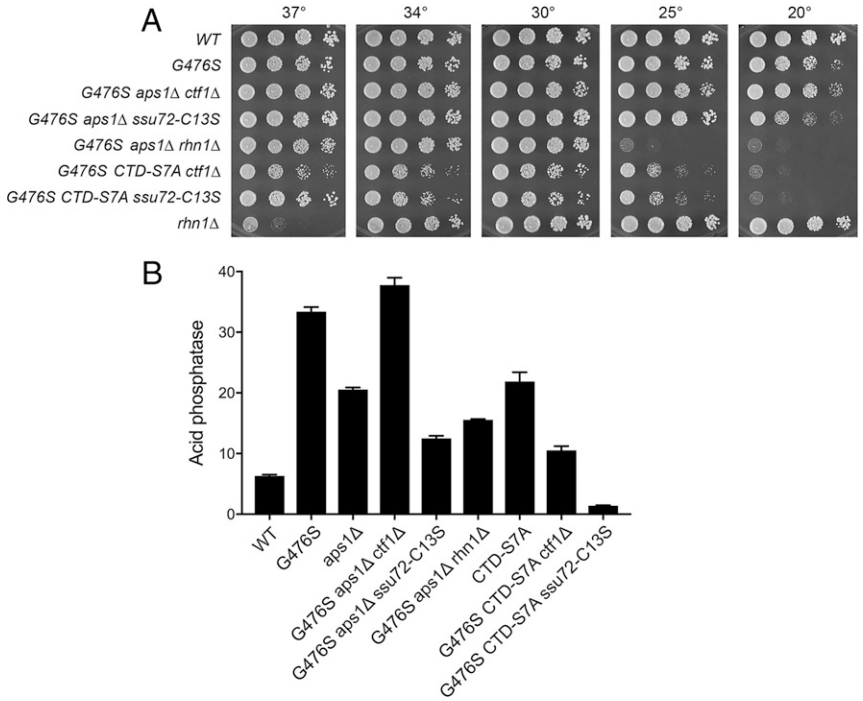

Fig. 7. Rescue of *seb1-G476S* synthetic lethality by CPF/Rhn1 mutations. (*A*) Strains with genotypes specified on the left were spot tested for growth on YES agar at the indicated temperatures. The *seb1-WT* and *seb1-G476S* alleles were marked with a 3′-flanking *hygMX* cassette. (*B*) Strains with genotypes specified on the *x*-axis were grown in liquid culture at 30 °C and assayed for acid phosphatase activity.

SI Appendix, Fig. S3 depicts 10 additional mRNAs in which the *seb1-G476S* allele elicits a shift in poly(A) site usage toward upstream sites within an mRNA 3′-UTR or the appearance of an upstream neo poly(A) site in the 3′-UTR. In some cases, the upstream shift in poly(A) site choice is appreciable in the total RNA-seq reads. For instance, wild-type cells make apparently equal use of two poly(A) sites in the *gms1* 3′-UTR, whereas *seb1-G476S* cells favor the use of a further upstream poly(A) site within the *gms1* 3′-UTR, apparently at the expense of the most distal site used in wild-type cells, which is reflected in a decrease in the RNA-seq read density over the distal 3′-UTR segment in *seb1-G476S* cells (*SI Appendix*, Fig. S3). Two upstream neo poly(A) sites in the *hhp1* 3′-UTR were detected in *seb1-G476S* cells, leading to a relative decrease in utilization of the distal poly(A) site predominant in wild-type cells and a relative decrease in RNA-seq reads over the distal *hhp1* 3′-UTR (*SI Appendix*, Fig. S3). Similar patterns of upstream shifts in poly(A) site choice and accompanying changes in distal 3′-UTR read density in *seb1-G476S* cells were observed for the *SPCC14G10.04*, *ado1*, and *pcl1* mRNAs (*SI Appendix*, Fig. S3).

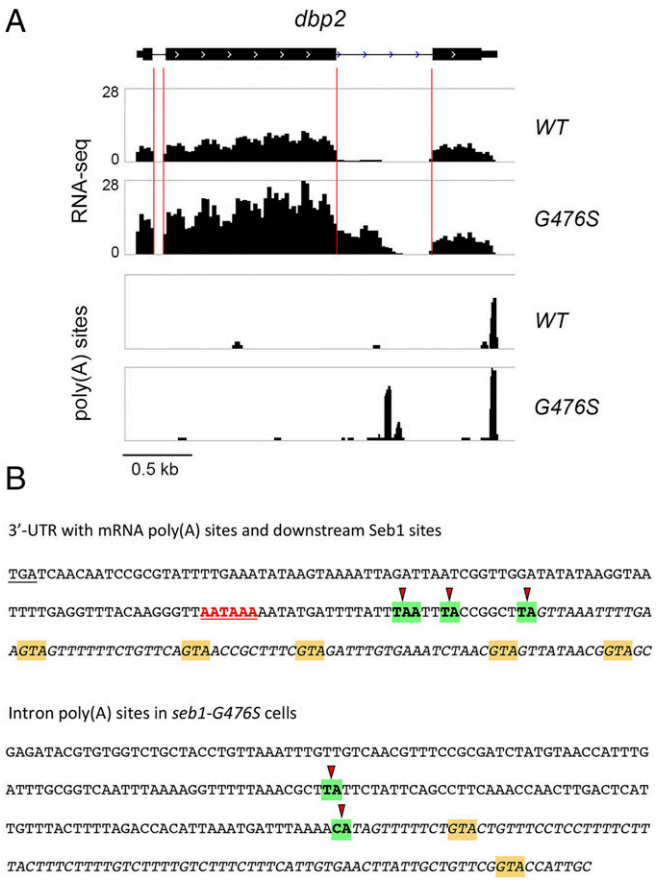

Fig. 8. *seb1-G476S* triggers utilization of an upstream intronic poly(A) site in the *dbp2* transcript. (*A*) Strand-specific RNA-seq read densities (*Top*; counts/base/million averaged in a 25-nt window) or poly(A) site-adjacent reads (*Bottom*; counts/base/million) of wild-type or *seb1-G476S* cells are plotted as a function of position across the *dbp2* chromosomal locus, which is depicted above the graphs with the three exons comprising the open reading frame denoted by thick bars, the two introns by thin lines, and the flanking UTRs by thin bars. The exon–intron boundaries in the RNA-seq profile are indicated by vertical red lines. The *x*-axis scale is shown on the bottom left. The RNA-seq read densities and poly(A) sites were determined from cumulative counts of three RNA-seq replicates. (*B*, *Top*) The DNA nucleotide sequence of the 3′-UTR is shown, starting from the *dbp2* TGA stop codon (underlined). Inspection of the poly(A) adjacent reads pinpointed three closely clustered cleavage/polyadenylation sites in the 3′-UTR, denoted in bold font and green shading. The poly(A) site cluster in the 3′-UTR is preceded by an AATAAA PAS (bold red font, underlined). The DNA sequence downstream of the distal poly(A) site is shown in italics and includes five GTA Seb1-binding motifs (shaded gold). (*Bottom*) Shown is the DNA sequence of the segment of the second *dbp2* intron surrounding the two neo poly(A) sites observed in *seb1-G476S* cells, neither of which is preceded by a hexanucleotide PAS. The DNA sequence downstream of the second intronic poly(A) site is shown in italics and includes two GTA Seb1-binding motifs (shaded gold). In both panels, the nucleotides adjacent to the poly(A) tails are indicated by a red triangle above the DNA sequence. Because the junction nucleotide is followed by one or two A nucleotides, the exact 3′-cleavage site within the green shaded elements is uncertain.

A Hypomorphic Loss-of-Function Seb1 Mutation Elicits Synergies Distinct from those of *seb1-G476S*. The *seb1-1* mutant (the first reported viable allele of *seb1*) was isolated from a mutagenized gene library by screening for a defect in RNA interference (RNAi)-independent pericentromeric heterochromatic silencing of a reporter gene system (35). The *seb1-1* allele has seven nucleotide mutations in the coding sequence, comprising three missense changes (G76S, R442G, and I524V) and four changes that did not alter the protein sequence; notably, the coding and noncoding changes were both necessary to attain the full *seb1-1* silencing defect and to confer a *ts* growth defect at 37 °C (35). Ensuing studies suggested the following: 1) Seb1 promotes Pol2 pausing that triggers heterochromatin formation; and 2) the *seb1-1* allele diminishes this activity of Seb1 (36). In effect, *seb1-1* behaves as a partial loss-of-function hypomorph, in which case the genetic interactions of *seb1-1* ought to be distinct from those of *seb1-G476S*, a *seb1* allele that we envision, based on the present studies, elicits a gain-of-function.

To address this issue, we crossed a *seb1-1* strain with the various *rpb1-CTD* and *CPF/Rhn1* mutants that had been tested for mutational synergies with *seb1-G476S*. With respect to the CTD mutants, *seb1-1* resembled *seb1-G476S* in that it was synthetically lethal with the *CTD-(S5•S5A)* and *CTD-(P6•P6A)* chimeras. However, in contrast to *seb1-G476S*, *seb1-1* was distinctively lethal in combination with *CTD-S2A*, barely viable in tandem with *CTD-Y1F*, sick at all temperatures when combined with *CTD-T4A*, and very sick at high temperatures in the *CTD-(P3•P3A)* background (*SI Appendix*, Fig. S4). Mutational synergies of *seb1-1* with *Y1F*, *S2A*, and *T4A* resonate with genetic evidence that Tyr1-Ser2-Thr4 form a three-letter CTD "word" that abets termination (12). It was of particular interest that the *CTD-S7A* allele overcame the *ts* phenotype of *seb1-1* and restored growth at 37 °C, while the *seb1-1* allele partially rescued the *cs* defect of *CTD-S7A* (*SI Appendix*, Fig. S4), i.e., a hypomorphic 3′-processing/termination defect of *seb1-1*, which becomes growth limiting at higher temperature, is countered by the precocious termination phenotype imputed to *CTD-S7A*.

In its genetic interactions with CPF and Rhn1, *seb1-1* differed from *seb1-G476S* in that *seb1-1* was synthetically lethal with *ctf1Δ* and *ssu72-C13S* (*SI Appendix*, Fig. S4). Combining *seb1-1* with *swd22Δ* and *ppn1Δ* resulted in failure to grow at 20 °C and 25 °C; *seb1-1 dis2Δ* cells displayed a less severe *cs* phenotype (*SI Appendix*, Fig. S4). We surmise that the residual function of the Seb1-1 mutant protein was more acutely dependent on the Ctf1 and Ssu72 components of the CPF core complex than on the three subunits that comprise the DPS module of the CPF holoassembly. There was no apparent mutational synergy between *seb1-1* and *rhn1Δ* with respect to growth on YES agar (*SI Appendix*, Fig. S4).

Discussion

The system of lncRNA-mediated transcriptional interference that underlies the repression of fission yeast phosphate homoeostasis gene *pho1* has proven to be a sensitive readout of genetic influences on 3′-processing/termination and a powerful tool for discovery of agents and regulators of this step of the Pol2 transcription cycle (9,

12, 14, 25, 37). The present identification of *seb1-G476S* in a genetic screen for relief of transcriptional interference highlights a unique mechanism by which Pol2 termination can be enhanced via a gain-of-function mutation in an essential termination factor, Seb1. The genetic and physical evidence for gain-of-function is copious and persuasive. To wit: 1) *seb1-G476S* de-represses *pho1* and *tgp1*, both of which are subject to lncRNA-mediated transcriptional interference; 2) RNA analysis shows that *seb1-G476S* elicits precocious lncRNA transcription termination in response to lncRNA 5′-proximal PASs; 3) *seb1-G476S* de-repression of *pho1* is erased by loss-of-function mutations in CPF subunits and Rhn1; 4) *seb1-G476S* suppresses the *ts* growth defect of *rhn1*Δ; and 5) *seb1-G476S* elicits an upstream shift in poly(A) site preference in several mRNA genes. To our knowledge, there is no prior example of a gain-of-function mutation in a eukaryal transcription termination protein. There is, however, precedent in bacteria, whereby Rho mutants were identified that were hyperactive in eliciting termination by *E. coli* RNA polymerase (38–40).

seb1-G476S displays a network of mechanistically informative genetic interactions with two other prominent governors of lncRNA interference with phosphate homeostasis genes: the Pol2 CTD and IPP dynamics. With respect to the CTD, *seb1-G476S* derepression of *pho1* is reversed by a T4A mutation, which prevents installation of the Thr4-PO_4 mark and is itself hyperrepressive of the *PHO* regulon. Substantial prior genetic evidence implicates Thr4-PO_4 as a positive effector of 3′-processing/termination, likely by virtue of Thr-PO_4 function as a component of the CTD-binding site for Seb1 and Rhn1 (12, 27, 41). More striking is the observation that *seb1-G476S* derepression of *pho1* is completely dependent on synthesis of IP8 by the Asp1 IPP kinase. IP8 is a metabolite agonist of 3′-processing/termination in fission yeast (25).

The mutational synergies and synthetic lethal genetic interactions of *seb1-G476S* make the case that the Seb1 gain-of-function in 3′-processing/termination is not restricted to the lncRNAs that control phosphate homeostasis genes (none of which are essential for fission yeast growth). *seb1-G476S* is synthetically very sick with the IPP pyrophosphatase-defective *asp1-H397A* allele, which raises the intracellular level of IP8 (23) and elicits a precocious lncRNA 3′-processing/termination phenotype similar to that of *seb1-G476S* (25). Combining the *seb1-G476S* and *asp1-H397A* alleles has an additive effect on the extent of *pho1* derepression. *seb1-G476S* is synthetically lethal in the absence of another IPP pyrophosphatase, Aps1. These results show that elevated IPP concentrations and increased termination activity of Seb1-G476S synergize to affect the 3′-processing/termination of one or more essential fission yeast genes. That the lethality of *seb1-G476S aps1Δ* is caused by overzealous 3′-processing/termination is nicely confirmed by our findings that viability of *seb1-G476S aps1Δ* cells is reinstated by loss-of-function mutations of CPF subunits Ctf1 and Ssu72 and of termination factor Rhn1. In the same vein, *seb1-G476S* is synthetically lethal with three CTD alleles—*S7A*, *S5•S5A*, and *P6•P6A*—each of which derepresses *pho1* in a manner dependent on CPF, Rhn1, and IP8 (12, 13, 30). The lethality of *seb1-G476S CTD-S7A* is overridden by Ctf1 and Ssu72 mutations, which signifies that *seb1-G476S* is contributing to a toxic phenotype of precocious termination. Finally, poly(A) site mapping fortifies the case for *seb1-G476S* as a gain-of-function in 3′-processing that favors the utilization of upstream poly(A) sites in mRNA genes that have alternative poly(A) sites or triggers the deployment of upstream poly(A) sites that were not evident in wild-type cells.

Clues to the mechanism by which *seb1-G476S* exerts its gain-of-function emerged from our crystal structure of the Seb1-G476S RNA-binding domain. The conformational change in the Ser476 mutant RRM vis-à-vis the wild-type RRM, entailing a 2.0- to 2.5-Å movement of the 11-aa loop from Val477 to Ser485, originates at the mutated amino acid and likely reflects the more restricted phi and psi angles available to serine (by virtue of its β-carbon) versus the less restricted Ramachandran plot unique to glycine. As yet, there has been no structure reported for Seb1 bound to RNA, and inference on that point could only be drawn by reference to the RNA complexes of the budding yeast Nrd1 RRM (29). In that regard, we could model the effect of the Ser476 mutation on RNA interaction by superimposing the shared 5′-GUA recognition element in the Nrd1 RRM structure on the Seb1-G476S RRM structure, which revealed the potential for new atomic contacts between the Ser476 and the uracil and guanine nucleobases of 5′-GUA. The predicted contacts of Ser476-Oγ are all within van der Waals distances of hydrogen-bonding atoms of the nucleobases. Taking into account that the RNA position/conformation might vary slightly between Nrd1 and Seb1, we envision that one or more of these atomic contacts will result in a gain of a hydrogen bond between Seb1 and RNA. Added van der Waals or hydrogen bond interactions might either enhance the interaction of Seb1 with consensus 5′-GUA target sites in nascent RNAs or confer interaction of new target sites that are not targets for wild-type Seb1 (e.g., 5′-GUG) by virtue of Ser476 donating a hydrogen bond to guanine-O6. We attempted to implement a gel shift assay to gauge the binding of purified wild-type and G476S RRM proteins to 5′ ^{32}P-labeled GUA-containing RNA oligonucleotides of varying length and flanking sequence context, but we were unable to detect a stable shifted species corresponding to an Seb1•RNA complex. The challenge now is to capture crystal structures of wild-type and mutant Seb1 RRMs in complex with RNA ligands, which will likely require a concerted effort at protein engineering to evade the favored crystal lattices that interfere with RNA binding.

Methods

The procedures for fission yeast growth and genetic manipulations, assays of cell surface acid phosphatase activity, whole genome sequencing, RNA-seq, poly(A) site mapping, Northern RNA analyses, and crystallographic structure determination are described in detail in *SI Appendix*. A list of fission yeast strains constructed for this study is compiled in *SI Appendix*, Table S4.

Data Availability. The RNA-seq data in this publication for the *seb1-G476S* strain and the control *seb1*$^{+}$ strain have been deposited in the National Center for Biotechnology Information's Gene Expression Omnibus (GEO) and are accessible through GEO Series accession number GSE168898. The Seb1 RRM-G476S crystal structure has been deposited in the PDB with identification code 7MI2. All other study data are included in the article and/or *SI Appendix*.

ACKNOWLEDGMENTS. We thank Hiten Madhani for the *seb1-1* strain. This work was supported by NIH Grants R01-GM134021 (B.S.) and R35-GM126945 (S.S.). The Memorial Sloan Kettering Cancer Center (MSKCC) Integrated Genomics Operation Core is funded by Cycle for Survival and the Marie-Josée and Henry R. Kravis Center for Molecular Oncology. The MSKCC structural biology core laboratory is supported by National Cancer Institute Grant P30-CA008748. X-ray diffraction data were collected at synchrotron facilities supported by grants and contracts from the NIH (P30-GM124165, HEI-S10OD021527) and the Department of Energy (DE-AC02-06CH11357). The funders had no role in study design, data collection and analysis, decision to publish, or preparation of the manuscript.

1. M. A. Cortazar *et al.*, Control of RNA Pol II speed by PNUTS-PP1 and Spt5 dephosphorylation facilitates termination by a "Sitting Duck Torpedo" mechanism. *Mol. Cell* **76**, 896–908.e4 (2019).
2. J. D. Eaton, L. Francis, L. Davidson, S. West, A unified allosteric/torpedo mechanism for transcriptional termination on human protein-coding genes. *Genes Dev.* **34**, 132–145 (2020).
3. N. J. Proudfoot, Transcriptional interference and termination between duplicated α-globin gene constructs suggests a novel mechanism for gene regulation. *Nature* **322**, 562–565 (1986).
4. J. E. Hirschman, K. J. Durbin, F. Winston, Genetic evidence for promoter competition in *Saccharomyces cerevisiae*. *Mol. Cell. Biol.* **8**, 4608–4615 (1988).

5. J. A. Martens, P. Y. Wu, F. Winston, Regulation of an intergenic transcript controls adjacent gene transcription in Saccharomyces cerevisiae. *Genes Dev.* **19**, 2695–2704 (2005).
6. I. Carter-O'Connell, M. T. Peel, D. D. Wykoff, E. K. O'Shea, Genome-wide characterization of the phosphate starvation response in *Schizosaccharomyces pombe*. *BMC Genomics* **13**, 697 (2012).
7. S. Shuman, Transcriptional interference at tandem lncRNA and protein-coding genes: An emerging theme in regulation of cellular nutrient homeostasis. *Nucleic Acids Res.* **48**, 8243–8254 (2020).
8. A. Garg, Y. Goldgur, B. Schwer, S. Shuman, Distinctive structural basis for DNA recognition by the fission yeast Zn_2Cys_6 transcription factor Pho7 and its role in phosphate homeostasis. *Nucleic Acids Res.* **46**, 11262–11273 (2018).
9. B. Schwer, A. M. Sanchez, S. Shuman, RNA polymerase II CTD phospho-sites Ser5 and Ser7 govern phosphate homeostasis in fission yeast. *RNA* **21**, 1770–1780 (2015).
10. D. Chatterjee, A. M. Sanchez, Y. Goldgur, S. Shuman, B. Schwer, Transcription of lncRNA *prt*, clustered *prt* RNA sites for Mmi1 binding, and RNA polymerase II CTD phospho-sites govern the repression of *pho1* gene expression under phosphate-replete conditions in fission yeast. *RNA* **22**, 1011–1025 (2016).
11. A. M. Sanchez, S. Shuman, B. Schwer, Poly(A) site choice and Pol2 CTD Serine-5 status govern lncRNA control of phosphate-responsive *tgp1* gene expression in fission yeast. *RNA* **24**, 237–250 (2018).
12. A. M. Sanchez, S. Shuman, B. Schwer, RNA polymerase II CTD interactome with 3′ processing and termination factors in fission yeast and its impact on phosphate homeostasis. *Proc. Natl. Acad. Sci. U.S.A.* **115**, E10652–E10661 (2018).
13. A. M. Sanchez, A. Garg, S. Shuman, B. Schwer, Genetic interactions and transcriptomics implicate fission yeast CTD prolyl isomerase Pin1 as an agent of RNA 3′ processing and transcription termination that functions via its effects on CTD phosphatase Ssu72. *Nucleic Acids Res.* **48**, 4811–4826 (2020).
14. B. Schwer, A. M. Sanchez, S. Shuman, Inactivation of fission yeast Erh1 de-represses *pho1* expression: Evidence that Erh1 is a negative regulator of *prt* lncRNA termination. *RNA* **26**, 1334–1344 (2020).
15. C. Yague-Sanz *et al*., Nutrient-dependent control of RNA polymerase II elongation rate regulates specific gene expression programs by alternative polyadenylation. *Genes Dev.* **34**, 883–897 (2020).
16. D. Eick, M. Geyer, The RNA polymerase II carboxy-terminal domain (CTD) code. *Chem. Rev.* **113**, 8456–8490 (2013).
17. J. L. Corden, RNA polymerase II C-terminal domain: Tethering transcription to transcript and template. *Chem. Rev.* **113**, 8423–8455 (2013).
18. K. M. Harlen, L. S. Churchman, The code and beyond: Transcription regulation by the RNA polymerase II carboxy-terminal domain. *Nat. Rev. Mol. Cell Biol.* **18**, 263–273 (2017).
19. B. Schwer, S. Shuman, Deciphering the RNA polymerase II CTD code in fission yeast. *Mol. Cell* **43**, 311–318 (2011).
20. V. Vanoosthuyse *et al*., CPF-associated phosphatase activity opposes condensin-mediated chromosome condensation. *PLoS Genet.* **10**, e1004415 (2014).
21. S. Wittmann *et al*., The conserved protein Seb1 drives transcription termination by binding RNA polymerase II and nascent RNA. *Nat. Commun.* **8**, 14861 (2017).
22. A. Garg, S. Shuman, B. Schwer, A genetic screen for suppressors of hyper-repression of the fission yeast *PHO* regulon by Pol2 CTD mutation T4A implicates inositol 1-pyrophosphates as agonists of precocious lncRNA transcription termination. *Nucleic Acids Res.* **48**, 10739–10752 (2020).
23. M. Pascual-Ortiz *et al*., Asp1 bifunctional activity modulates spindle function via controlling cellular inositol pyrophosphate levels in *Schizosaccharomyces pombe*. *Mol. Cell. Biol.* **38**, e00047-e18 (2018).
24. D. E. Dollins *et al*., Vip1 is a kinase and pyrophosphatase switch that regulates inositol diphosphate signaling. *Proc. Natl. Acad. Sci. U.S.A.* **117**, 9356–9364 (2020).
25. A. M. Sanchez, A. Garg, S. Shuman, B. Schwer, Inositol pyrophosphates impact phosphate homeostasis via modulation of RNA 3′ processing and transcription termination. *Nucleic Acids Res.* **47**, 8452–8469 (2019).
26. H. Mitsuzawa, E. Kanda, A. Ishihama, Rpb7 subunit of RNA polymerase II interacts with an RNA-binding protein involved in processing of transcripts. *Nucleic Acids Res.* **31**, 4696–4701 (2003).
27. T. Kecman *et al*., Elongation/termination factor exchange mediated by PP1 phosphatase orchestrates transcription termination. *Cell Rep.* **25**, 259–269.e5 (2018).
28. J. F. Lemay *et al*., The Nrd1-like protein Seb1 coordinates cotranscriptional 3′ end processing and polyadenylation site selection. *Genes Dev.* **30**, 1558–1572 (2016).
29. E. Franco-Echevarría *et al*., The structure of transcription termination factor Nrd1 reveals an original mode for GUAA recognition. *Nucleic Acids Res.* **45**, 10293–10305 (2017).
30. A. Garg, A. M. Sanchez, B. Schwer, S. Shuman, Transcriptional profiling of fission yeast RNA polymerase II CTD mutants. *RNA* **27**, 560–570 (2021).
31. S. T. Safrany *et al*., The diadenosine hexaphosphate hydrolases from *Schizosaccharomyces pombe* and *Saccharomyces cerevisiae* are homologues of the human diphosphoinositol polyphosphate phosphohydrolase. Overlapping substrate specificities in a MutT-type protein. *J. Biol. Chem.* **274**, 21735–21740 (1999).
32. R. S. Kilari, J. D. Weaver, S. B. Shears, S. T. Safrany, Understanding inositol pyrophosphate metabolism and function: Kinetic characterization of the DIPPs. *FEBS Lett.* **587**, 3464–3470 (2013).
33. J. Mata, Genome-wide mapping of polyadenylation sites in fission yeast reveals widespread alternative polyadenylation. *RNA Biol.* **10**, 1407–1414 (2013).
34. M. Schlackow *et al*., Genome-wide analysis of poly(A) site selection in *Schizosaccharomyces pombe*. *RNA* **19**, 1617–1631 (2013).
35. D. B. Marina, S. Shankar, P. Natarajan, K. J. Finn, H. D. Madhani, A conserved ncRNA-binding protein recruits silencing factors to heterochromatin through an RNAi-independent mechanism. *Genes Dev.* **27**, 1851–1856 (2013).
36. J. Y. Parsa, S. Boudoukha, J. Burke, C. Homer, H. D. Madhani, Polymerase pausing induced by sequence-specific RNA-binding protein drives heterochromatin assembly. *Genes Dev.* **32**, 953–964 (2018).
37. T. C. Henry *et al*., Systematic screen of *Schizosaccharomyces pombe* deletion collection uncovers parallel evolution of the phosphate signal transduction pathway in yeasts. *Eukaryot. Cell* **10**, 198–206 (2011).
38. N. Tsurushita, M. Hirano, K. Shigesada, M. Imai, Isolation and characterization of *rho* mutants of *Escherichia coli* with increased transcription termination activities. *Mol. Gen. Genet.* **196**, 458–464 (1984).
39. N. Tsurushita, K. Shigesada, M. Imai, Mutant rho factors with increased transcription termination activities. I. Functional correlations of the primary and secondary polynucleotide binding sites with the efficiency and site-selectivity of rho-dependent termination. *J. Mol. Biol.* **210**, 23–37 (1989).
40. H. Mori, M. Imai, K. Shigesada, Mutant rho factors with increased transcription termination activities. II. Identification and functional dissection of amino acid changes. *J. Mol. Biol.* **210**, 39–49 (1989).
41. O. Jasnovidova, M. Krejcikova, K. Kubicek, R. Stefl, Structural insight into recognition of phosphorylated threonine-4 of RNA polymerase II C-terminal domain by Rtt103p. *EMBO Rep.* **18**, 906–913 (2017).